Journal of Materials Chemistry A

PAPER

View Article Online
View Journal | View Issue

Cite this: J. Mater. Chem. A, 2018, 6, 10755

Preventing lithium dendrite-related electrical shorting in rechargeable batteries by coating separator with a Li-killing additive

Sheng S. Zhang, *[a] Xiulin Fan [b] and Chunsheng Wang [b]

Dendritic electrodeposition is an intrinsic feature of Li metal, and Li dendrite-related electrical shorting is a major cause of thermal runaway in Li metal batteries. In order to prevent such electrical shorting, a Li-killing layer consisting of TiO_2 nanoparticles embedded in a porous Kynar polymer matrix is coated onto one side of a conventional Celgard separator and faced to the cathode. After filling with liquid electrolyte, the Kynar polymer swells to a gel while TiO_2 serves as a Li-killer by reacting with the Li dendrites that penetrate through the separator. Additionally, the Li-killing layer increases the thermal dimensional stability of the separator, and the wettability, uptake and uphold of the liquid electrolyte. It is shown that a Li/Cu cell with the Li-killing layer does not undergo electrical shorting even if the Li metal is entirely plated onto the counter electrode, whereas an identical cell using a pristine separator rapidly experiences shorting. Moreover, the Li-killing layer increases the rate capability and capacity retention of a $Li/LiNi_{0.80}Mn_{0.10}Co_{0.10}O_2$ cell. Impedance analysis reveals that such improvements are attributed to increased electrolyte uptake and uphold, which consequently reduces the solid electrolyte interphase resistance and charger-transfer resistance.

Received 27th March 2018
Accepted 10th May 2018

DOI: 10.1039/c8ta02804d

rsc.li/materials-a

Introduction

Lithium metal is recognized to be an ideal anode material for high energy density batteries because of its high specific capacity (3861 mA h g^{-1}) and low redox potential (−3.0401 V *vs.* standard hydrogen electrode). However, commercializing lithium metal batteries has been hampered by the inferior cycling efficiency and poor safety of the Li metal anode, which are related to the growth of Li dendrites.[1–4] The deposition and growth of Li dendrites are neither predictable nor controllable, and Li dendrite-related electrical shorting is known to be a major cause of thermal runaway in batteries, not only in Li metal batteries but also in Li-ion batteries. It is common for Li metal to become directly plated onto the graphite anode when Li-ion batteries are charged at high rate or at low temperature,[5,6] especially when the batteries are overcharged.[7] Furthermore, Li dendrite-related electrical shorting takes place not only in liquid electrolyte batteries, but also in solid electrolyte batteries. It has been reported that Li dendrites can grow along the grain boundaries of a solid state electrolyte and eventually penetrate through the solid electrolyte membrane, resulting in electrical shorting.[8,9] To date, there have been no works in which a Li foil was entirely plated onto the counter electrode without electrical shorting, although so-called "Li dendrite-free" strategies have been frequently reported in many recent publications. Developing a separator capable of killing the Li dendrites may be a more viable strategy for preventing the Li dendrite-related electrical shorting.

Ceramic materials are of particular significance in battery applications. For microporous polyolefin separators, coating with ceramic particles increases the thermal dimensional stability and electrolyte uptake of the separators.[10–14] For poly (ethylene oxide) based solid polymer electrolytes, adding ceramic fillers reduces the crystallinity of poly(ethylene oxide) and consequently increases the ionic conductivity of the polymer electrolytes.[15–17] For gel polymer electrolytes, adding ceramic particles as a filler enhances not only the dimensional stability of the electrolyte membrane but also the uptake and uphold of liquid electrolytes.[18–21] Beside the above benefits, some ceramic particles such as $AlPO_4$ have been shown to increase the Li^+ ion transference number and stabilize the Li-electrolyte interface, enabling smooth and efficient Li deposition.[22] In battery applications, Al_2O_3,[16,20,21,23] SiO_2,[11,15,18,24,25] and TiO_2 [12–14,17] micro- or nano-particles have been the most intensively studied due to their low cost and easy preparation. Of particular interest, it was reported that SiO_2 in nano-particle size can be electrochemically reduced, and that sandwiching SiO_2 nanoparticles between two separators can extend the cycle life of a Li metal battery by reacting with the Li dendrites that penetrate through the separator.[26] Compared with SiO_2, TiO_2 is

[a]Electrochemistry Branch, RDRL-SED-C, Sensors and Electron Devices Directorate, U.S. Army Research Laboratory, Adelphi, MD 20783-1138, USA. E-mail: shengshui.zhang.civ@mail.mil; shengshui@gmail.com

[b]Department of Chemical and Biomolecular Engineering, University of Maryland, College Park, MD 20742, USA

more reactive with Li metal, and more importantly the reaction produces a variety of low conductive lithiated titanium oxides, as suggested by the Li–Ti–O ternary phase diagram.[27] Moreover, the redox potentials of TiO_2 are in a range lower than 2 V *vs.* Li/Li^+,[28,29] which is beyond those of most cathode materials currently used in Li-ion batteries. In other words, contact between TiO_2 and the cathode will not affect the cathode's electrochemical performance. Taking the above knowledge into account, we herein coated a highly porous TiO_2–Kynar composite layer onto one side of a conventional Celgard separator, and placed the composite layer facing the cathode. Upon filling with the liquid electrolyte, the Kynar polymer swells, forming a TiO_2–Kynar based composite gel polymer electrolyte (CGPE), while the TiO_2 particles act to kill the Li dendrites that penetrate through the separator, and consequently prevent the Li dendrite-related electrical shorting. In this paper, the effect of the TiO_2–Kynar composite layer on the thermal dimensional stability of the separator, the wettability of the liquid electrolyte, and the cycling performance of the $Li/LiNi_{0.80}Mn_{0.10}Co_{0.10}O_2$ cell will be discussed in addition to the unique capability of TiO_2 particles to eliminate Li dendrite-related electrical shorting.

Experimental

Titanium oxide (TiO_2) nanopowder (Sigma-Aldrich) and poly (vinylidene fluoride-*co*-hexafluoropropylene) (Kynar FLEX 2822, Arkema) were used as received. The cathode material, $LiNi_{0.80}Mn_{0.10}Co_{0.10}O_2$ (NMC), was provided by Targray, Canada. A highly porous TiO_2–Kynar composite layer was coated onto one side of a Celgard 2325 membrane by the phase inversion method according to the following procedures. First, TiO_2 and Kynar powders were mixed in a 1 : 1 weight ratio and added into a 95 : 5 (wt) mixed solvent of acetone and deionized water, followed by vigorously stirring at 50 °C for 2 h to obtain a homogeneous suspension. Then, the warm suspension was coated onto one side of the Celgard 2325 membrane, and the solvent was allowed to evaporate in air (*i.e.*, the phase inversion process) to form a highly porous TiO_2–Kynar composite layer on the separator. For simplicity, the TiO_2–Kynar composite coated separator is referred to as the T-separator, and the pristine Celgard 2325 membrane is referred to as the P-separator. Prior to use, both separators were dried at 60 °C overnight under vacuum. In order to examine the reaction of TiO_2 with Li metal, the same TiO_2–Kynar suspension was coated onto a Cu foil and the resulting Cu foil was used as the Li plating substrate in a Li/Cu cell. An NMC cathode was prepared by coating a slurry consisting of 80% NMC, 10% Super-P carbon black and 10% poly(vinylidene fluoride) binder in *N*-methyl pyrrolidinone onto an Al foil. The resultant cathode was punched onto circular disks with a 1.27 cm^2 area, and dried at 110 °C under vacuum for 16 h. The NMC loading of the cathode was 5.0–5.5 mg cm^{-2} on average.

The morphology of the separator and electrode was observed on a scanning electron microscope (SEM, Hitachi SU-70). The wettability of the separators was tested by selecting propylene carbonate (PC) as the high polar solvent and triglyme as the low polar solvent. The solvent uptake and porosity of the separator were calculated based on the change of weight before and after fully absorbing the triglyme solvent.

A solution of 1.0 mol kg^{-1} $LiFP_6$ dissolved in a 3 : 7 (wt) mixture of ethylene carbonate and ethyl methyl carbonate was used as the liquid electrolyte. Using the separators and electrodes described above, various types of BR2335 coin cells were assembled, and cycled on a Maccor Series 4000 tester under the conditions noted in either the figures or figure captions. Before testing, the cells were heated at 60 °C for 1 h so as to turn the porous Kynar polymer matrix into a gel. The rate capability of the Li/NMC cells was evaluated by charging galvanostatically at 1C to 4.2 V, followed by holding the voltage at 4.2 V until the current declined to 0.1C, where the C rate was referred to the specific capacity of a 150 mA h g^{-1} NMC. The ac-impedance of the cells was measured at open-circuit voltage using a Solartron SI 1260 Impedance/Gain-Phase Analyzer in combination with a Solartron SI 1287 Electrochemical Interface in the frequency range from 1.0×10^5 Hz to 0.01 Hz and an ac oscillation of 10 mV amplitude. All impedances were measured at 20 °C.

Results and discussion

Fig. 1 shows SEM images of the P-separator and T-separator. The P-separator is a polypropylene (PP) monolayer membrane made by a dry process, whose pores are highly oriented to the machine direction of the uniaxial stretching process, as indicated by an arrow in Fig. 1a. The surface of the T-separator (Fig. 1b) is fully covered by the porous TiO_2–Kynar composite. A detailed view (Fig. 1c) shows that the composites are highly porous, with the TiO_2 nanoparticles embedded in the highly porous Kynar polymer matrix. This feature is attributed to the phase inversion process induced by the faster evaporation rate of acetone (solvent) than water (antisolvent), which produces highly porous polymer structures.[30] After cycling (that is, the separator was subject to a heating process at 60 °C for 1 h), the porous polymer structures are no longer present. Instead, the polymer is plasticized by the liquid electrolyte to an SEM-

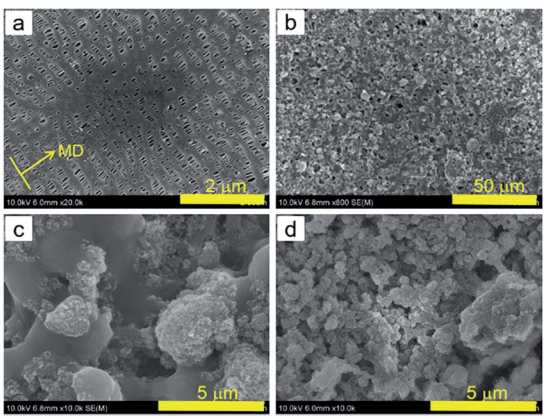

Fig. 1 SEM image of the surfaces of the separators. (a) P-separator, (b) T-separator, (c) T-separator in detail, and (d) T-separator after 1 cycle in a Li/Cu cell.

invisible gel that intimately binds the TiO_2 particles together. The above observations suggest that the highly porous structure of the TiO_2–Kynar composite can facilitate the filling of the cell with liquid electrolyte, and that the CGPE can be *in situ* formed after the cell is activated by the liquid electrolyte and heated at elevated temperature for a short time period.

The thermal dimensional stability of the separators was visually assessed after the separators were stored in a hot oven for a certain time period. Fig. 2 compares digital photos of the P-separator and T-separator having the composite loading of ~1.8 mg cm^{-2} before and after being stored at 130 °C and 160 °C, respectively, for 1 h. PP materials generally have a melting point range from 160 to 166 °C. After storing at 130 °C (below PP's melting point), the P-separator was still white in color, suggesting that the porous structure still remained. After storing at 160 °C (near PP's melting point), the P-separator turned transparent, indicating that all the pores were closed. While it was not expected to affect the extent of pore-closing in the separators, the TiO_2–Kynar composite greatly stabilized the dimension of the separators. It can be observed from Fig. 2 that at both temperatures, both separators shrank and the shrinkage was highly oriented to the machine direction as indicated by the arrows, being highly consistent with the pore orientation as shown in Fig. 1a. However, the T-separator experienced much less shrinkage as compared with the P-separator. This is because the relatively rigid TiO_2–Kynar composite acts as a mechanical skeleton enhancing the separator's dimensional stability.

The wettability of the separators was examined by using two types of solvent, *i.e.*, one high polar solvent and one low polar solvent. For the high polar solvent (propylene carbonate, Fig. 3a), the P-separator could not be wetted at all, even after being heated at 80 °C for 30 min, due to the nonpolar nature of the PP material. In contrast, the T-separator was wetted immediately, which is attributed to two properties of the TiO_2–Kynar composite: (1) the highly porous structure and (2) the superhydrophilicity of TiO_2 particles.[31] After heating at 80 °C for 30 min, the color of the T-separator changed from white to

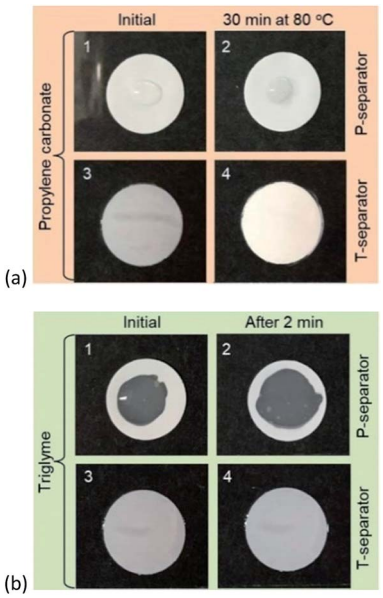

Fig. 3 Comparison of the wettability of P-separator and T-separator. (a) High polar propylene carbonate solvent, and (b) low polar triglyme solvent.

super white, which reflects a change in the state of the propylene carbonate solvent from liquid droplets immobilized in pores to molecules plasticized into the Kynar polymer matrix (*i.e.* forming a transparent gel with Kynar polymer). For the low polar solvent (triglyme, Fig. 3b), the P-separator was wetted slowly while the T-separator was wetted instantly, having no visible difference compared with that observed in the case of propylene carbonate. The above results reveal that the highly porous TiO_2–Kynar composite not only facilitates the wetting of the separator with liquid electrolyte but also *in situ* forms a CGPE with the liquid electrolyte when heated at elevated temperature for a short time period.

The solvent uptake and composite porosity of the T-separator were further evaluated by using triglyme. Fig. 4

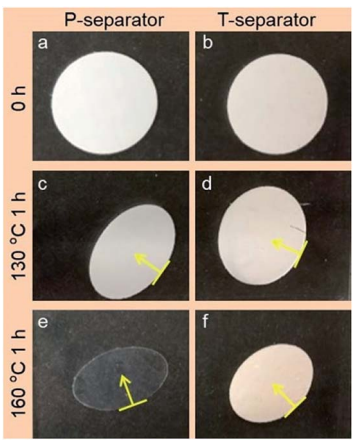

Fig. 2 Digital photos of P-separator (left column) and T-separator (right column) before and after being heated at different temperatures for 1 h, in which the arrows indicate the machine direction.

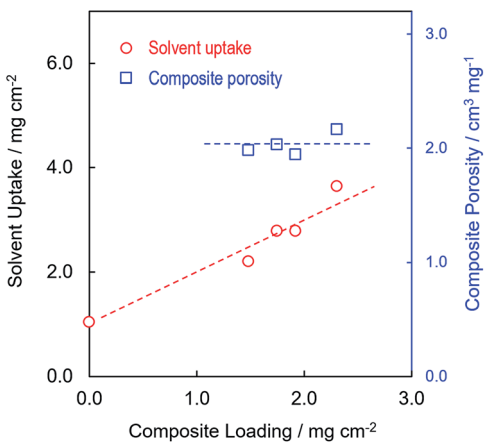

Fig. 4 Correlation of the solvent uptake of T-separator and the porosity of the TiO_2–Kynar composite layer with the loading of composite.

depicts the correlation of solvent uptake and composite porosity with the loading of TiO_2–Kynar composite. It can be seen that the P-separator (*i.e.* the one with zero loading) had a solvent uptake of 1.0 mg cm^{-2}, and that the solvent uptake increased linearly with the loading of composite. In contrast, the porosity of the composite constantly remained at ~2.1 cm^3 mg^{-1}, regardless of the composite loading. In other words, the porosity is purely associated with the composition of the TiO_2–Kynar composite and the parameters of the phase inversion, such as the ratio of solvent to antisolvent and the evaporating rate of the solvents.

As demonstrated above, the TiO_2–Kynar composite can be *in situ* converted to CGPE by absorbing liquid electrolyte and heating at elevated temperature for a short time period. Therefore, the resistance of the CGPE-coated separator was measured and compared with that of the electrolyte-wetted P-separator. Fig. 5a compares the impedance spectra of the two separators, in which the CGPE-coated separator was *in situ* formed from a T-separator with a composite loading of ~1.8 mg cm^{-2} by absorbing liquid electrolyte and heating at 80 °C for 30 min. It is observed that the resistance of the CGPE-coated separator lies between those of one and two electrolyte-wetted P-separators. This is understandable because the CGPE, which is equivalent to an extra resistance, is connected in series to the separator. On the other hand, Fig. 5b compares the impedance spectra of two Li/NMC cells with a P-separator and a T-separator, respectively. In general, the impedance spectra of Li metal batteries are composed of two compressed semi-circles, which respectively reflect the resistance of the solid electrolyte interphase (SEI) of the electrodes (R_{SEI}) and the charge-transfer resistance of the two electrode–electrolyte interfaces (R_{ct}),[32,33] as described by the equivalent circuit shown in the inset of Fig. 5b. Regardless of the state-of-charge, the cell with a T-separator has higher bulk resistance (R_b). However, it has much smaller R_{SEI} and R_{ct}, which consequently leads to lower overall impedance as compared with that using a P-separator. The above results indicate that the CGPE formed by the TiO_2–Kynar composite not only increases the ionic conductivity of the SEI at the cathode but also facilitates the kinetics of the cathode reaction, both of which are attributed to the increased electrolyte uptake.

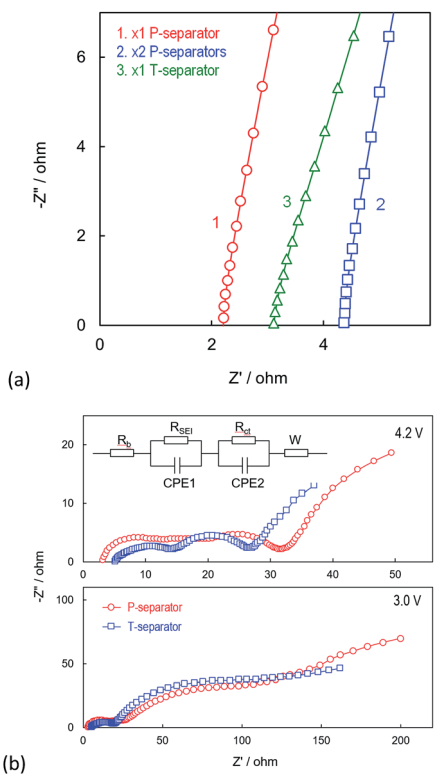

Fig. 5 (a) Impedance spectra of symmetric SS/electrolyte/SS cells with different separators, and (b) comparison of the impedance spectra of Li/NMC cells with P-separator and T-separator, respectively, at charged (4.2 V) and discharged (3.0 V) states. Note that "SS" represents stainless steel electrode.

The primary purpose of this work is to validate the feasibility of TiO_2 as a killer of Li dendrites. In order to examine the ability of TiO_2 to react with Li metal, the TiO_2–Kynar composite was coated onto a Cu foil, and the resulting Cu foil was used as the Li plating substrate in a Li/Cu cell. The voltage profile of the initial Li plating period up to a capacity of 2.0 mA h cm^{-2} is illustrated in Fig. 6, in which the two insets show photos of the TiO_2–Kynar composite before and after Li plating. It can be observed that initial capacities of 0.46 mA h cm^{-2} are obtained above 0 V *vs.* Li/Li^+. These capacities are attributed to the electrochemical reduction (*i.e.*, lithiation) of TiO_2, which can be briefly expressed by eqn (1).

$$xLi^+ + TiO_2 + xe^- \rightarrow Li_xTiO_2 \quad (1)$$

Due to the absence of conductive carbon in the TiO_2–Kynar composite layer, the reduction voltage of TiO_2 is considerably lower than the ~1.8 V of the regular Li/TiO_2 cells[28,29] as a result of the high polarization. Additionally, the change in the color of the TiO_2 particles from white to black further confirms that the TiO_2 particles were electrochemically lithiated in this experiment. Moreover, comparing Fig. 1c and d indicates that the TiO_2 particles became slightly bigger after the Li/Cu cell was plated and stripped for one cycle, providing further evidence for the electrochemical lithiation of the TiO_2 nanoparticles.

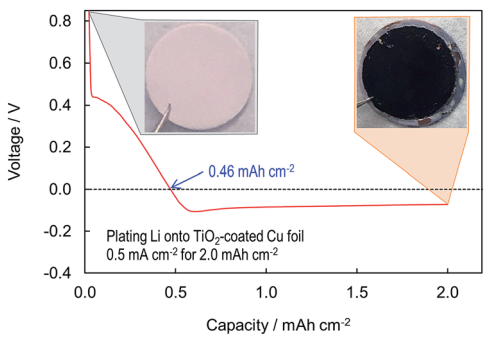

Fig. 6 Voltage profile of the initial Li plating on a TiO_2–Kynar composite coated Cu foil, in which the two insets show photos of the TiO_2–Kynar composite layer before and after Li plating.

Unlike the case of a Li/TiO_2 cell, prevention of the Li dendrite-related electrical shorting in batteries must be implemented through chemical lithiation of TiO_2. In order to examine the chemical lithiation, combination of a P-separator and a T-separator with the TiO_2–Kynar composite layer facing the P-separator was used in the Li/Cu cell. In this way, neither the Li anode nor the Cu electrode was in contact with the TiO_2 particles. For fair comparison, a pair of P-separators was used in a control cell. Fig. 7 shows the voltage profile of these two Li/Cu cells when plating Li at 1.0 mA cm^{-2} until the cell underwent electrical shorting by the Li dendrites or the Li metal was completely plated onto the counter electrode. It can be seen that the control cell (curve-a) suffered local shorting at 11.9 h as indicated by arrow 1, which worsened with increasing Li plating time, and the cell completely failed at 32.9 h, as indicated by arrow 2, at which time the cell's voltage sharply rose to 0 V. In addition, there was an unusual decrease in the Li plating voltage before the cell underwent local shorting, corresponding to an increase in the polarization during the time period from 7.8 h to 11.9 h. This is because in this period, the accumulation of Li dendrites became loose, which aggravated the reaction of the Li dendrites with the electrolyte solvents as a result of an increase in the specific surface area of the mossy Li whiskers, and consequently increased the resistance of the Li deposits. In contrast, the voltage of the cell with a P-separator and a T-separator (curve-b) remained stable at 60–65 mV until the Li metal was completely plated onto the Cu side, as indicated by arrow 3, showing that the cell's voltage abruptly decreased at around 117 h. The above results verify that the TiO_2 particles are able to kill Li dendrites by chemical reaction with Li metal, and that our proposal is practically feasible for preventing the Li dendrite-related electrical shorting.

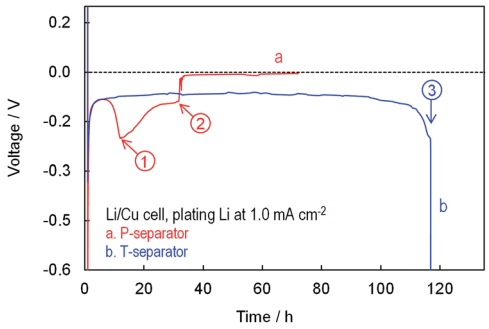

Fig. 7 Voltage profile of Li plating onto Cu foil at 1.0 mA cm^{-2} until the cell undergoes electrical shorting by Li dendrites or Li metal is completely plated onto the Cu side. (a) Two P-separators, and (b) combination of a P-separator and a T-separator with the TiO_2–Kynar composite layer facing the P-separator.

The effect of the TiO_2–Kynar composite layer on the cell's performances in Li/NMC cells was evaluated, as presented in Fig. 8. In order to avoid irreversible structural degradation of the $LiNi_{0.80}Mn_{0.10}Co_{0.10}O_2$ cathode material, the charging voltage of the cells was kept at no higher than 4.3 V as suggested by the previous literature.[34] In the first cycle (Fig. 8a), the cell with the P-separator and the cell with the T-separator had nearly the same discharge capacity (159–161 mA h g^{-1}) and coulombic efficiency (82–83%). However, the cell with the T-separator had slightly smaller polarization, especially in the initial period of the first charging. Fig. 8b shows that the cell with the T-separator exhibited normal rate capability behaviour. That is, the capacity decreased and the polarization increased with an increase in the current rate. The effect of the separators on the rate capability is shown in Fig. 8c. When the current rate was lower than 3C, the two cells had the same capacities. When the

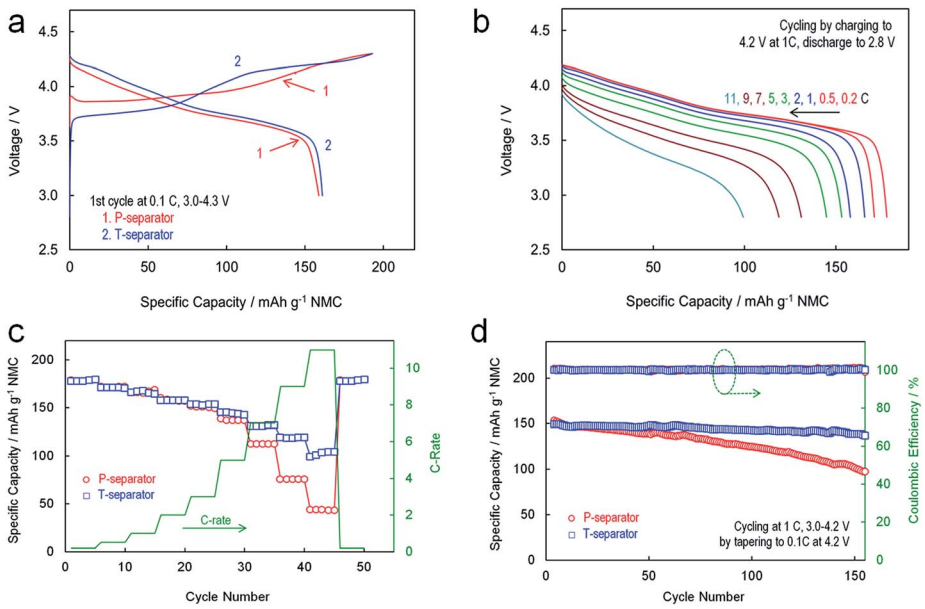

Fig. 8 Cycling performance of the Li/NMC cells with P-separator and T-separator, respectively. (a) Voltage profile of the 1st cycle, (b) discharging voltage profile of the cell with T-separator at different current rates, (c) rate capability cycling between 2.8 V and 4.2 V, and (d) capacity retention and coulombic efficiency.

current rate reached or exceeded 5C, however, the capacity of the cell with the T-separator became higher, and the capacity gap between the two cells was widened as the current rate increased. This observation is in good agreement with the results of impedance analysis as shown in Fig. 5b, that is, the cell with the T-separator had lower overall impedance as compared with the one employing the P-separator. Beside the better rate capability, the cell with the T-separator further demonstrated more stable capacity retention as illustrated in Fig. 8d. The above improvements can be attributed to the better electrolyte uptake and uphold of the T-separator. As demonstrated above, the TiO_2–Kynar composite on the T-separator can be *in situ* converted to a CGPE, in which both the TiO_2 particles and Kynar polymer matrix increase the uptake and uphold of liquid electrolyte.

Conclusions

In summary, we proposed and demonstrated a simple and practically viable approach for preventing the Li dendrite-related electrical shorting by coating a highly porous TiO_2–Kynar composite layer onto one side of a conventional Celgard separator and placing the TiO_2 composite layer on the cathode side. In addition to offering the desired functionality, the TiO_2–Kynar composite layer also increases the thermal dimensional stability and electrolyte wettability of the separator. The TiO_2–Kynar composite can be *in situ* converted to a CGPE after filling the cell with liquid electrolyte and heating the cell at elevated temperature for a short time period. The resulting CGPE is capable of killing Li dendrites by chemical reaction of TiO_2 particles with the Li dendrites that penetrate through the separator. Furthermore, the CGPE is beneficial to the rate capability and capacity retention of the Li/NMC cells by increasing the uptake and uphold of the liquid electrolyte. The results of this work indicate that modification of the existing separators with a Li-killing additive would be a simple and feasible approach for preventing the Li dendrite-related electrical shorting.

Conflicts of interest

There are no conflicts of interest to declare.

Acknowledgements

The authors are grateful to Dr A. von Cresce for providing NMC cathode material, and to Dr C. Lundgren for her critical reading of the manuscript and valuable comments.

References

1 W. Xu, J. Wang, F. Ding, X. Chen, E. Nasybulin, Y. Zhang and J. G. Zhang, *Energy Environ. Sci.*, 2014, **7**, 513–537.
2 D. C. Lin, Y. Y. Liu and Y. Cui, *Nat. Nanotechnol.*, 2017, **12**, 194–206.
3 X. B. Cheng, R. Zhang, C. Z. Zhao and Q. Zhang, *Chem. Rev.*, 2017, **117**, 10403–10473.
4 S. S. Zhang, *ACS Appl. Energy Mater.*, 2018, **1**, 910–920.
5 S. S. Zhang, *J. Power Sources*, 2006, **161**, 1385–1391.
6 M. Petzl, M. Kasper and M. A. Danzer, *J. Power Sources*, 2015, **275**, 799–807.
7 W. Lu, C. M. Lopez, N. Liu, J. T. Vaughey, A. Jansen and D. W. Dees, *J. Electrochem. Soc.*, 2012, **159**, A566–A570.
8 E. J. Cheng, A. Sharafi and J. Sakamoto, *Electrochim. Acta*, 2017, **223**, 85–91.
9 F. Aguesse, W. Manalastas, L. Buannic, J. M. Lopez del Amo, G. Singh, A. Llordes and J. Kilner, *ACS Appl. Mater. Interfaces*, 2017, **9**, 3808–3816.
10 S. S. Zhang, *J. Power Sources*, 2007, **164**, 351–364.
11 X. Zhu, X. Jiang, X. Ai, H. Yang and Y. Cao, *ACS Appl. Mater. Interfaces*, 2015, **7**, 24119–24126.
12 R. S. Juang, C. T. Hsieh, P. A. Chen and Y. F. Chen, *J. Power Sources*, 2015, **286**, 526–533.
13 X. Zhu, X. Jiang, X. Ai, H. Yang and Y. Cao, *J. Membr. Sci.*, 2016, **504**, 97–103.
14 Y. Xi, P. Zhang, H. Zhang, Z. Wan, W. Tu and H. Tang, *Int. J. Electrochem. Sci.*, 2017, **12**, 5421–5430.
15 L. Fan, C. W. Nan and S. Zhao, *Solid State Ionics*, 2003, **164**, 81–86.
16 S. K. Fullerton-Shirey and J. K. Maranas, *J. Phys. Chem. C*, 2010, **114**, 9196–9206.
17 P. K. Singh, B. Bhattacharya and R. K. Nagarale, *J. Appl. Polym. Sci.*, 2010, **118**, 2976–2980.
18 X. W. Zhang, Y. Li, S. A. Khan and P. S. Fedkiw, *J. Electrochem. Soc.*, 2004, **151**, A1257–A1263.
19 J. Manuel, Y. Liu, M. H. Lee, X. Zhao, M. Kim, G. S. Chauhan, H. J. Ahn and J. H. Ahn, *Sci. Adv. Mater.*, 2016, **8**, 741–748.
20 X. Wang, H. Zhu, G. M. A. Girard, R. Yunis, D. R. MacFarlane, D. Mecerreyes, A. J. Bhattacharyya, P. C. Howlett and M. Forsyth, *J. Mater. Chem. A*, 2017, **5**, 23844–23852.
21 V. Vishwakarma and A. Jain, *J. Power Sources*, 2017, **362**, 219–227.
22 X. X. Zeng, Y. X. Yin, Y. Shi, X. D. Zhang, H. R. Yao, R. Wen, X. W. Wu and Y. G. Guo, *Chem*, 2018, **4**, 298–307.
23 K. W. Kim, H. W. Kim, Y. Kim and J. K. Kim, *Electrochim. Acta*, 2017, **236**, 394–398.
24 P. F. R. Ortega, J. P. C. Trigueiro, G. G. Silva and R. L. Lavall, *Electrochim. Acta*, 2016, **188**, 809–817.
25 B. Kurc, *Electrochim. Acta*, 2016, **190**, 780–789.
26 K. Liu, D. Zhuo, H. W. Lee, W. Liu, D. Lin, Y. Lu and Y. Cui, *Adv. Mater.*, 2017, **29**, 1603987.
27 H. Kleykamp, *Fusion Eng. Des.*, 2002, **61–62**, 361–366.
28 K. Saravanan, K. Ananthanarayanan and P. Balaya, *Energy Environ. Sci.*, 2010, **3**, 939–948.
29 H. Tao, M. Zhou, K. Wang, S. Cheng and K. Jiang, *Sci. Rep.*, 2017, **7**, 43895.
30 H. Strathmann and K. Kock, *Desalination*, 1977, **21**, 241–255.
31 K. R. Arturi, H. Jepsen, J. N. Callsen, E. G. Sogaard and M. E. Simonsen, *Prog. Org. Coat.*, 2016, **90**, 132–138.
32 S. S. Zhang, K. Xu and T. R. Jow, *J. Electrochem. Soc.*, 2002, **149**, A1521–A1526.
33 S. S. Zhang, K. Xu and T. R. Jow, *Electrochem. Solid-State Lett.*, 2002, **5**, A92–A94.
34 J. Li, L. E. Downie, L. Ma, W. Qiu and J. R. Dahn, *J. Electrochem. Soc.*, 2015, **162**, A1401–A1408.

